Notes

Contribution from the Laboratoire de Chimie de la Matière Condensée (UA 302, CNRS) and Laboratoire de Chimie Organique Industrielle (UA 403, CNRS), Ecole Nationale Superieure de Chimie, 11 rue P. et M. Curie, 75005 Paris, France, and Department of Chemistry, University of Groningen, Nijenborgh 16, 9747 AG Groningen, The Netherlands

ENDOR Spectroscopy of (Pentamethylcyclopentadienyl)(cyclooctatetraene)zirconium, $[\{\eta^5\text{-}(CH_3)_5C_5\}Zr(\eta^8\text{-}C_8H_8)]$: The First Stable Paramagnetic Zirconium Sandwich Compound

Didier Gourier,*,† Edmond Samuel,‡ and Jan H. Teuben§

Received May 10, 1989

A variety of zirconium(III) cyclopentadienyl complexes have been identified in solution by using EPR spectroscopy. However, practically none of them so far could be isolated and characterized as such in the solid form. This was ascribed to their inherent kinetic instability,[1] in contrast with complexes of Ti(III) of the same family.

It is well-known that, in the case of the electron-deficient group 4 metal complexes, a sandwich-like structure can be stabilized by η^7- or η^8-coordination with cycloheptatrienyl or cyclooctatetraene ligands.[2,3] In the case of Zr, the diamagnetic compound [CpZr(cht)] was isolated[4] and its crystal structure established.[5] However, the 17-electron [CpZr(cot)] analogue remains unknown to this day although a number of diamagnetic zirconium compounds containing the (cot) ligand have been prepared. With the Cp* ligand, the compound [Cp*Zr(cot)] was successfully isolated.[6] The crystal structure confirmed the anticipated planar bonding of both rings to the central metal.[7] This is to our knowledge the first stable and well-characterized paramagnetic Zr sandwich compound that retains its structure and properties in the solid phase as well as in solution. For this reason, we undertook the present study in order to determine by EPR and ENDOR spectroscopy the metal and ligand contributions to the configuration of its electronic ground state; a similar investigation using both techniques has already been performed on a similar sandwich compound, the [CpTi(cht)] anion.[8]

Experimental Section

[Cp*Zr(cot)] was synthesized as described earlier.[6] All manipulations were performed under argon. Toluene was used as solvent, and solutions were sealed in quartz tubes under vacuum for EPR and ENDOR experiments. Toluene was also used as solvent for optical absorption measurements. EPR and ENDOR spectra were recorded with a Bruker ER 220 D X-band spectrometer equipped with an Aspect 2000 monitored ENDOR unit. A radiofrequency power of 100 W was used for all the ENDOR spectra.

Temperatures between 10 and 100 K were obtained with an ESR 9 helium flow cryostat from Oxford Instruments. Optical absorption spectra were measured at room temperature with a Uvikon 860 spectrometer.

Abbreviations used in this paper: Cp* = $[\eta^5\text{-}(CH_3)_5C_5]$; (cot) = $(\eta^8\text{-}C_8H_8)$; (cht) = $(\eta^7\text{-}C_7H_7)$.

Results

Electron Paramagnetic Resonance. At room temperature, the EPR spectrum is composed of an isotropic line at g_{iso} = 1.9738

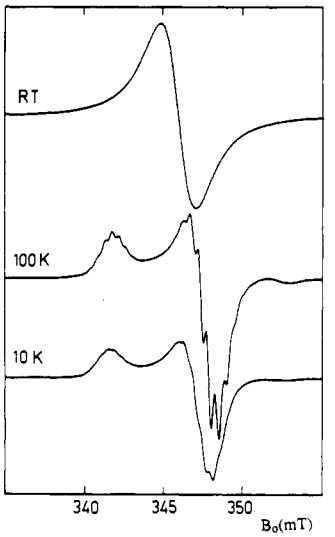

Figure 1. EPR spectra of [Cp*Zr(cot)] in toluene solution.

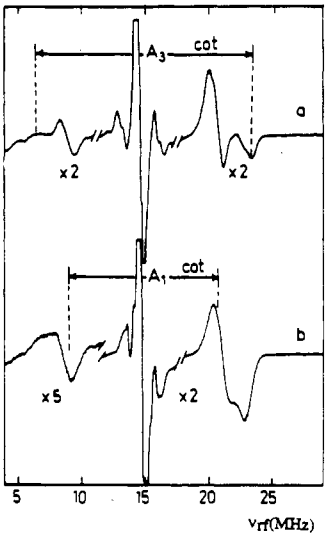

Figure 2. ENDOR spectra of [Cp*Zr(cot)] recorded at 10 K (microwave power 12.6 mW; modulation 50 kHz). Magnetic field setting: (a) B_0 = 343.6 mT; (b) B_0 = 347.6 mT.

without a resolved structure (Figure 1). At 100 K in frozen solution the spectrum exhibits a typical powder line shape with two components reflecting the axial symmetry of the molecule, $g_\parallel$ = 1.9989 and $g_\perp$ = 1.9612. The spectrum also shows a well-resolved hyperfine (hf) interaction with protons of the (cot) ring. The good resolution is due to the free rotation of this (cot) ring at 100 K, which partially averages the hf interaction. At

† Laboratoire de Chimie de la Matière Condensée.
‡ Laboratoire de Chimie Organométallique.
§ University of Groningen.

(1) Cardin, D. J.; Lappert, M. F.; Raston, C. L. *The Chemistry of Organozirconium and -hafnium Compounds*; Ellis Howard Ltd.: London, 1986; Chapter 13.
(2) Zeinstra, J. D.; de Boer, J. L. *J. Organomet. Chem.* **1973**, *54*, 207.
(3) Kroon, P. A.; Helmholdt, R. B. *J. Organomet. Chem.* **1970**, *25*, 451.
(4) Van Oven, H. O.; Groenenboom, C. J.; de Liefde Meijer, H. J. *J. Organomet. Chem.* **1974**, *81*, 379.
(5) Rogers, R. D.; Teuben, J. H. *J. Organomet. Chem.* **1988**, *354*, 169.
(6) Blenkers, J.; Bruin, P.; Teuben, J. H. *J. Organomet. Chem.* **1985**, *297*, 61.
(7) Rogers, R.; Teuben, J. H. *J. Organomet. Chem.* **1984**, *359*, 41.
(8) Gourier, D.; Samuel, E. *Inorg. Chem.* **1988**, *27*, 3018.

0020-1669/89/1328-4663$01.50/0

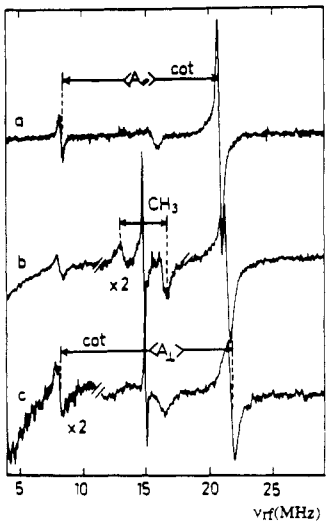

Figure 3. ENDOR spectra of [Cp*Zr(cot)] recorded at 100 K (microwave power 200 mW; modulation 50 kHz). Magnetic field setting: (a) B_0 = 342.1 mT; (b) B_0 = 346.1 mT; (c) B_0 = 348.6 mT.

10 K, the EPR spectrum is similar except that the hf interaction with the (cot) ring is hardly detectable because of the frozen ring motion at this temperature. It is noteworthy that the hf interaction with ^{91}Zr nuclei (11.2% natural abundance, $I = {}^5/_2$) is not resolved within the temperature range 10 K to room temperature. This is most probably due to structural disorder,[7] which is known to produce a M_I-dependent broadening of hyperfine lines.

Electron Nuclear Double Resonance (ENDOR). Two examples of ENDOR spectra recorded at 10 K are shown in Figure 2. They exhibit three distinct features: (i) a strong line with more or less resolved structure, located at the nuclear proton fequency ν_p, which is due to purely dipolar interactions with protons of solvent molecules (matrix ENDOR line); on both sides, (ii) a doublet of lines separated by 3 MHz, with a resolved structure dependent on the magnetic field setting B_0, due to the interaction with Cp* methyl protons and (iii) two doublets of lines having a typical powder line shape, the positions of which also depend on B_0, due to the interaction with protons of (cot) rings.

At 100 K, the ENDOR spectra are significantly modified (Figure 3), because of the onset of intramolecular motions, although the solvent is still frozen at this temperature. (i) The matrix ENDOR is strongly reduced and is now represented by a weak and extremely sharp line at ν_p (Figure 3b) and disappears when the magnetic field B_0 is set on the parallel component of the EPR spectrum (Figure 3a). This behavior reflects the libration of solvent molecules. (ii) The (Cp*) ENDOR lines are weak, but remain almost similar in shape to those observed at 10 K. (iii) Interactions with protons of (cot) rings are now represented by one single pair of lines with a symmetrical (single crystallike) line shape. This particular line shape reflects the motion of (cot) rings around the molecular axis.

ENDOR of (η^8-C_8H_8) Protons. The shape of the EPR spectrum is determined at 10 and 100 K by the anisotropy of the axial g tensor. When the magnetic field is set at a value B_0 for an ENDOR measurement, one saturates only spin packets occurring at this field, and in turn, one selects only a given set of molecules with axes making an angle θ with the field direction. At 10 K, the rings are motionless so that, for a given molecular orientation θ, the protons can assume all the positions around the molecular axis. Furthermore, the principal axis (A_3 axis) of the proton hf interaction being almost colinear to the zirconium–proton direction, it makes an angle θ_N with the molecular axis. As a consequence, the selection of molecular orientation does not imply the selection of a proton orientation, and even if the selected angle is equal to θ_N, the angles between the magnetic field direction and all the Zr–H directions can assume all the values between 0 and $2\theta_N$. This is the reason for the powder line shape of the ENDOR spectra recorded at 10 K (Figure 2). Generally, if the magnetic field is characterized by polar angles θ and ϕ with the z axis (molecular axis) and the x axis, the ENDOR frequencies are given by the following expression:[9]

$$\nu(m_s) = \left[\sum_{i=1}^{3}\left(\frac{m_s g_i}{g}A_i h_i - h_i \nu_p\right)^2\right]^{1/2} \quad (1)$$

where h_i is the direction cosine between the magnetic field and the ith hyperfine tensor axis. The proton hyperfine interaction is composed of the isotropic part A_{iso}, which is positive for these kinds of sandwich compounds,[10] and the traceless dipolar part A_i^{dip}.

$$A_i = A_{iso} + A_i^{dip} \qquad A_{iso} = \frac{1}{3}\sum_{i=1}^{3} A_i \quad (2)$$

Since A_3^{dip} is always positive for protons, the largest value of the hf tensor is given by A_3. Measurement of A_3 was made by recording the ENDOR spectrum at different magnetic field settings. More precisely, a stepwise variation of B_0 across the EPR spectrum results in an increasing separation between the outermost pair of ENDOR lines. For B_0 = 345.5 mT, this separation is a maximum which means that the selected angle θ satisfies the equality $\theta = \theta_N$ (Figure 2a). In that case the direction cosines are $h_3 = 1$ and $h_1 = h_2 = 0$ for the set of protons giving the ENDOR lines and expression 1 reduces to $\nu(m_s) = |m_s A_3 - \nu_p|$ for the two extreme lines separated by $A_3 = +16.70 \pm 0.05$ MHz.

One of the two other hf tensor axes (chosen to be the A_1 axis) is parallel to the ring plane[10] and thus perpendicular to the molecular axis. A_1 can be measured by setting B_0 at the high-field flank of the EPR spectrum, which corresponds to the selection of molecules with $\theta = \pi/2$. In that case, we obtain $h_3 = h_2 = 0$ and $h_1 = 1$ for one set of protons, and the two ENDOR lines occur at frequencies $\nu(m_s) = |m_s A_1 - \nu_p|$. The spectrum shown in Figure 2b, recorded with B_0 = 347.5 mT, gives $|A_1| = 11.10 \pm 0.05$ MHz. The sign of A depends on the relative magnitude of A_{iso} and A_1^{dip}.

The other hf parameters of (cot) can be measured by using the ENDOR spectra recorded at 100 K. At this temperature, the ring motion around the molecular axis is rapid and the dipolar part A_{dip} of the hf tensor is partially averaged. The motionally averaged hf tensor $\langle \mathbf{A} \rangle$ has now an axial symmetry with two components $\langle A_\parallel \rangle$ and $\langle A_\perp \rangle$, and the symmetry axis (which is the rotation axis) is colinear to the molecular axis. $\langle A_\parallel \rangle$ and $\langle A_\perp \rangle$ are related to the static hf components A_i by

$$\begin{aligned} \langle A_\parallel \rangle &= A_2 \sin^2 \theta_N + A_3 \cos^2 \theta_N \\ \langle A_\perp \rangle &= {}^1/_2(A_2 \cos^2 \theta_N + A_1 + A_3 \sin^2 \theta_N) \end{aligned} \quad (3)$$

$\langle A_\parallel \rangle$ and $\langle A_\perp \rangle$ can be accurately measured because the ENDOR lines are narrow and symmetrical. In the case of coaxial **g** and hf tensors axes, expression 1 gives

$$\nu(m_s) = \left[\left(\frac{m_s}{g} g_\parallel \langle A_\parallel \rangle - \nu_p\right)^2 \cos^2 \theta + \left(\frac{m_s}{g} g_\perp \langle A_\perp \rangle - \nu_p\right)^2 \sin^2 \theta\right]^{1/2} \quad (4)$$

When the magnetic field is set at the low- and high-field flanks of the EPR spectrum, the selected angles are $\theta = 0$ and $\theta = \pi/2$ and the ENDOR frequencies in expression 4 are respectively $\nu(m_s) = |m_s \langle A_\parallel \rangle - \nu_p|$ and $\nu(m_s) = |m_s \langle A_\perp \rangle - \nu_p|$ with $\langle A_\parallel \rangle = +12.2$ (9) MHz and $\langle A_\perp \rangle = +13.5$ (1) MHz.

The value $A_{iso} = +13.1$ (0) MHz for the isotropic hf interaction is obtained from expressions 2 and 3:

$$A_{iso} = {}^1/_3(\langle A_\parallel \rangle + 2\langle A_\perp \rangle) \quad (5)$$

It should be noticed that $\langle A_\parallel \rangle$ and $\langle A_\perp \rangle$ have been taken positive, as in the analogous Ti sandwich compounds, because other combinations of signs give either a negative value for A_{iso} or a value $A_{iso} = +4.91$ MHz. The latter is too small and is not compatible with the line shape of the room-temperature EPR spectrum, which

(9) Brown, T. G.; Hoffman, B. M. *Mol. Phys.* **1980**, *39*, 1073.
(10) Wolf, R.; Schweiger, A.; Gunthard, H. *Mol. Phys.* **1984**, *53*, 567.

Table I. EPR and ENDOR Parameters for the Title Compound[a]

(cot) protons	$g_\parallel$	1.9989
	$g_\perp$	1.9612
	$\langle A_\parallel \rangle$	+12.2 (9)
	$\langle A_\perp \rangle$	+13.5 (1)
	A_{iso}	+13.1 (0)
	A_3	+16.70 ± 0.05
	A_2	+11.10 ± 0.05
	A_1	+11.50 ± 0.05
methyl protons	$A_\parallel$	−2.40 ± 0.05
	$A_\perp$	−3.60 ± 0.03
	A_{iso}	−3.2

[a] Hyperfine interactions are given in MHz.

is only determined by the isotropic interaction with the (cot) ring.

Having obtained a precise value for A_{iso}, one can show that A_1 is positive and the third value A_i of the hf tensor can thus be obtained by using expression 2. All the results are gathered in Table I.

If we assume that the anisotropic part of the hf interaction is of a purely dipole–dipole nature, the component A_3^{dip} is related to R_N by the point dipole–dipole expression $A_3^{dip} = 2g\beta g_N\beta_N R_N^{-3}$. ENDOR data give $R_N = 3.50$ Å. A crystallographic structure[7] showed that the (cot) ring possesses two stable orientations labeled "a" (36% occupancy) and "b" (64% occupancy). The Zr–C(η_8) distances are slightly different for the two orientations, and if we assume a C–H distance of 1.08 Å, the two Zr–H distances are $R_N = 3.32$ and 3.36 Å in configurations "a" and "b", respectively. These values are slightly lower than those measured by ENDOR. The discrepancy is probably not due to inaccuracies in our measurements because even if twe assume that configuration "b" is predominant, the value of A_3 calculated by using X-ray data amounts to 17.23 MHz by using the value $A_{iso} = 13.10$ MHz. This value is 0.53 MHz higher than the experimental one, which largely exceeds the experimental uncertainty. The major source of discrepancy should rather be a contribution of a small spin density in the π ($2p_z$) orbitals of carbon atoms, which should be responsible for a small deviation from the pure point dipole–dipole model.[10] For configuration "a", calculation of A_3 gives $A_3 = 17.20$ MHz, which differs from that calculated for configuration "b" only by 0.03 MHz. This difference lies within our experimental uncertainty, and we may conclude that structural disorder has no observable effect on the ENDOR spectra at 10 K.

ENDOR of (η^5-Me_5C_5) Protons. Comparison of ENDOR spectra recorded at 100 and 10 K allowed us also to obtain the principal values of the hf tensor for the methyl protons. Let us first consider the methyl ENDOR lines at 100 K (Figure 3). The signal to noise ratio is quite low, but the matrix ENDOR line is strongly reduced so that it does not overlap with the methyl ENDOR line. It should be first noticed that these lines are dissymmetrical, with powder type line shape, contrary to the single ENDOR lines of (cot) protons. The powder line shape means that rotation of the Cp* ring is hindered by the presence of the methyl groups. This quenching of ring motion by methyl groups has already been observed in [(Me-Cp)Ti(cot)] by ENDOR spectroscopy.[11] Stepwise variation of B_0 across the EPR spectrum allows one to measure the highest value for the hf interaction, $|A_{max}| = 3.6$ MHz. It should be noticed that this value does not correspond to one of the principal values of the hf tensor of a fixed methyl proton since the dipolar interaction is partially averaged by the rotation of the methyl groups around the C–C bonds. The low signal to noise ratio does not allow us to measure $|A_{min}|$ at this temperature, although it appears that this anisotropy is evidently small, as expected for hf interactions with methyl protons.[12]

Figure 4 shows some representative spectra recorded at 10 K in the frequency range of matrix and methyl ENDOR. The highest value for the methyl hf interaction, $|A_{max}| = 3.60 \pm 0.03$ MHz, is equal to that measured at 100 K. This indicates that the methyl groups are still rotating around the C–C bonds at 10 K. Despite the low temperature, this is not unexpected because of the low activation energy for methyl rotation. The other hf coupling value is found to be $|A_{min}| = 2.40 \pm 0.05$ MHz.

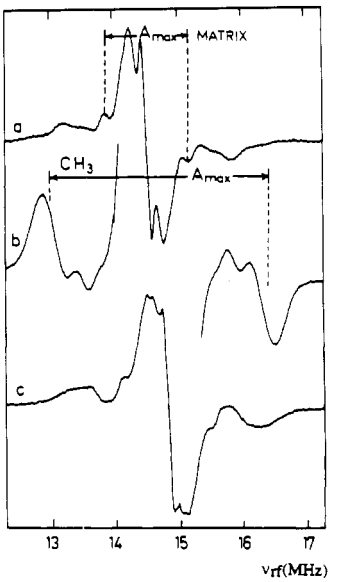

Figure 4. ENDOR spectra of [Cp*Zr(cot)] recorded at 10 K in the region of CH_3 with matrix resonance (microwave power 12.6 mW; modulation 20 kHz). Magnetic field setting: (a) $B_0 = 340.6$ mT; (b) $B_0 = 344.6$ mT; (c) $B_0 = 348.1$ mT.

The assignment of A_{max} and A_{min} to the components $A_\parallel$ and $A_\perp$ of the hf tensor can be made from line-shape considerations. For an axial or pseudoaxial hf tensor, the perpendicular component of the ENDOR spectrum is always stronger than the parallel one. This can be seen for example in Figure 2 for the ENDOR of (cot) protons. Since the ENDOR lines giving $|A_{max}|$ are more intense than those giving $|A_{min}|$, we conclude that they correspond respectively to $|A_\perp|$ and $|A_\parallel|$. The signs of the hf parameters can be obtained by considering the expressions $A_\parallel = A_{iso} + 2A_{dip}$ and $A_\perp = A_{iso} - A_{dip}$.

Since A_{dip} is positive for a point dipole–dipole interaction, the inequality $|A_\parallel| < |A_\perp|$ implies that A_{iso} is negative and hence $A_\perp = -3.60 \pm 0.03$ MHz, but the sign of $A_\parallel$ is not determined. The two possible values for the dipolar part of the hf tensor are $A_{dip} = +0.4$ MHz and $A_{dip} = +2$ MHz for $A_\parallel < 0$ and $A_\parallel > 0$, respectively. The second value is much too high if we consider that A_{dip} is averaged by the methyl rotation. It is known that, for freely rotating methyl groups in organic radicals, the anisotropy of the hf tensor is only about $0.1A_{iso}$, which clearly corresponds to $A_\parallel < 0$. Using these values, the isotropic part of the hf tensor is found to be $A_{iso} = -3.2$ MHz.

The matrix ENDOR line exhibits a partially resolved structure as shown in Figure 4. This structure is due to purely dipole–dipole interactions with protons of nearest solvent molecules. The shape of the matrix ENDOR slightly varies with the magnetic field setting, which is due to the nonspherical symmetry of the solvent cages. The highest coupling with solvent protons occurs when B_0 is set at the low-field side of the EPR spectrum (Figure 4a). This shows that the nearest solvent molecules are located along the molecular axis. The two ENDOR lines, separated by 1.32 MHz, occur at frequencies $\nu = \nu_p \pm g\beta g_N\beta_N R^{-3}$ where $R = 4.9$ Å is the zirconium–solvent proton distance.

Optical Absorption. The optical absorption (OA) spectrum was recorded in the 300–900-nm range. It is dominated by strong absorptions in the near-UV region so that absorption bands in the visible region are not well resolved. However, the compound under study is not stable, and experimental evidence shows that the decomposition products do not absorb in the visible region. The OA in the near-UV region appears to be only slightly affected by decomposition so that spectral substraction reveals the structure of the absorption bands in the visible region. Figure 5 shows the

(11) Gourier, D.; Samuel, E. *J. Am. Chem. Soc.* **1987**, *109*, 4571.
(12) Kurreck, H.; Kirste, B.; Lubitz, W. *Electron Nuclear Resonance Spectroscopy of Radicals in Solution*; VCH Publishers: New York, 1988.

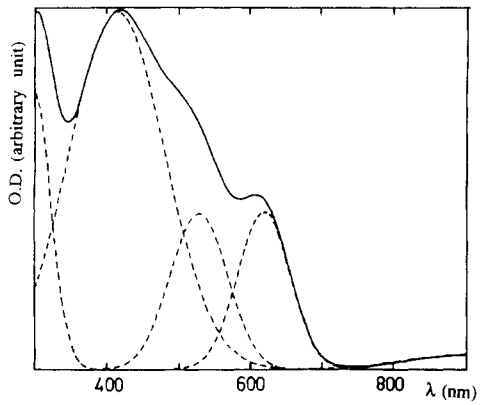

Figure 5. Optical absorption spectrum of [Cp*Zr(cot)] at room temperature in toluene obtained after substraction of the spectrum recorded at t = 20 mn from the spectrum recorded at t = 0, immediately after dissolution (full line). The spectrum is accurately reproduced by the sum of three Gaussian bands (dashed lines).

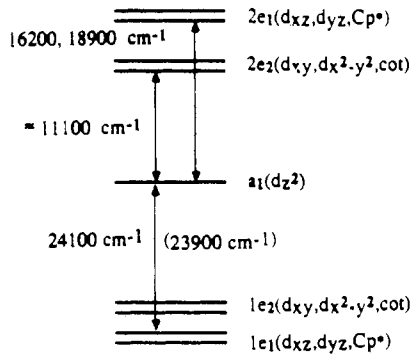

Figure 6. Schematic energy level diagram of [Cp*Zr(cot)] deduced from optical absorption. The energy separation (in parentheses) is deduced from UPS measurements.[13]

results obtained after substraction of the OA spectrum recorded after 20 min of decomposition from that recorded immediately after dissolution of the compound. By this method, the absorption in the near-UV region is strongly attenuated. The spectrum can be accurately simulated by the sum of four Gaussian bands peaking at 415 nm (24 100 cm^{-1}; ϵ = 900), 528 nm (18 900 cm^{-1}; ϵ = 450), 618 nm (16 200 cm^{-1}; ϵ = 450), and about 900 nm (11 100 cm^{-1}; ϵ = 45). Photoelectron spectroscopy[13] showed that the energy separation between the $1e_1$ and $1e_2$ orbitals (which are accidentally degenerate) and the $1a_1$ ground-state orbital is 23 900 cm^{-1}. The strong transition at 415 nm is thus attributed to the $^2A_1(1e_2^4,1e_1^4,a_1) \rightarrow {}^2E_1(1e_2^4,1e_1^3,a_1^2)$ transition from the filled $1e_1$ orbitals to the a_1 orbital (Figure 6). The three other transitions are due to electron excitation from a_1 to empty $2e_1$ and $2e_2$ orbitals. It should be noticed that the $^2A_1(1e_2^4,1e_1^4,a_1) \rightarrow {}^2E_2(1e_2^4,1e_1^4,2e_2)$ transition is forbidden in both C_5 and C_8 symmetries, so that it would correspond to the OA band near 900 nm. The two other bands at 528 and 618 nm have nearly equal intensities and widths and should correspond to similar transitions. They could likely correspond to the symmetry-allowed transition $^2A_1(1e_2^4,1e_1^4,a_1) \rightarrow {}^2E_1(1e_2^4,1e_1^4,2e_1)$ split by a static distortion of less than 3000 cm^{-1} (Figure 6). In fact, such splitting is expected because the centroid–Zr–centroid angle is 174° instead of 180°.[7] Such splitting should also be observable for the $^2A_1 \rightarrow {}^2E_1$ bands at 415 nm. However, its width is 4 times that of the $^2A_1 \rightarrow {}^2E_1$ bands at 528 and 618 nm, and the lack of splitting could be due to the fact that the width of two individual components (due to the electron–vibration coupling) is larger than the crystal field splitting.

Discussion

In the parent compound [CpTi(cot)], titanium–Cp bonding takes place through electron donation from e_1(Cp) filled orbitals to empty $3d\pi(d_{xz},d_{yz})$ metal orbitals, and titanium–(cot) bonding involves electron donation from e_2(cot) filled orbitals to empty $3d\delta(d_{xy},d_{x^2-y^2})$ metal orbitals. The bonding e_2 and e_1 orbitals contain only 19% and 8.5% metal 3d character respectively, so that $3d\pi$ and $3d\delta$ metal orbitals are essentially antibonding. The $a_1(d_{z^2})$ metal orbital, which contains the unpaired electron, is essentially nonbonding. These bonding characteristics are also expected to apply to [Cp*Zr(cot)].

The structure of [Cp*Zr(cot)] electron ground state can be obtained from EPR and ENDOR, which give the metal and ligand characters of the orbital ground state. Spin densities in ligand orbitals can be derived from hf parameters. The isotropic interaction with (cot) protons, A_{iso}, is related to the spin density, ρ_H, at protons by the expression

$$A_{iso} = \frac{8\pi}{3} g\beta g_N \beta_N |\psi_0(s)|^2 \rho_H \qquad (6)$$

Experimental results give ρ_H(cot) = $+9.2 \times 10^{-3}$ and $\rho_H(CH_3)$ = -2.3×10^{-3} for (cot) and methyl, respectively. The positive spin density at (cot) protons is due to direct delocalization of the unpaired electron spin on the 1s hydrogen orbitals of (cot) hydrogens. It is noteworthy that this value is larger than the spin density ρ_H(cot) = $+6.2 \times 10^{-3}$ found in CpTi(cot), although the metal–proton distance is smaller in [CpTi(cot)] (3.19 Å) than in [Cp*Zr(cot)] (3.34 Å). The large distance in the latter compound reveals a weaker interaction between e_2(cot) and $4d\delta$ metal orbitals of zirconium while the higher spin density reveals a better overlap of the $a_1(4d_{z^2})$ zirconium orbital with the 1s hydrogen orbital than in the case of $3d_{z^2}$ with titanium. Concerning the Zr–(cot) fragment, the electron ground state is thus less nonbonding in [Cp*Zr(cot)] than in [CpTi(cot)].

The spin density at methyl protons cannot be ascribed to a direct delocalization as with (cot) protons because its sign is negative. This means that the isotropic hf interaction with methyl protons is indirect, via a Zr–C_{cp}–Me fragment. It is known that if there is a finite spin density in a $\pi(2p_z)$ orbital of the carbon adjacent to methyl group, the hyperconjugation mechanism results in a spin density at methyl protons, leading to an isotropic hf interaction given by the McConnell relation $A_{iso} = Q_{Me}\rho_\pi$, where Q_{Me} = 56–98 MHz for aromatic compounds.[14] From our ENDOR data we obtain ρ_π = $(-3$ to $-6) \times 10^{-2}$ at $\pi(2p_z)$ orbitals of Cp carbon atoms. A finite spin density certainly also exists at $\pi(2p_z)$ orbitals of (cot) carbon atoms, but is more difficult to evaluate. It should slightly affect the isotropic hf interaction via a spin polarization of the σ_{CH} bond and the dipolar interaction. The negative value of ρ_π found for Cp carbons is very similar to that predicted and measured in dibenzene vanadium[10,15] ($\rho_\pi = -2.7 \times 10^{-2}$), which confirms the nonbonding character of the electron ground state in [Cp*Zr(cot)]. For an electron ground state with a bonding character, the direct delocalization of the unpaired electron on $\pi(2p_z)$ orbitals of rings should give a positive spin density. The negative spin density found experimentally is due to a spin polarization of the lower e_1 orbitals.

The g shifts are related to the metal character of the electron ground state and are due to spin–orbit admixture of excited states into the ground state. The $g_\parallel$ value is very close to the free-electron spin g value, which confirms that the metal orbital of the ground state is of purely d_{z^2} character. The $g_\perp$ value is due to spin–orbit admixture of $1e_1$ and $2e_1$ states into the ground state (see Figure 6). Simple calculations give

$$g_\perp = g_e - 6\lambda_{eff}a^2\left[\frac{b^2}{E(1e_1) - E(a_1)} + \frac{c^2}{E(2e_1) - E(a_1)}\right] \qquad (7)$$

where the coefficients a, b, and c are the coefficients of 3d metal orbitals in a_1, $1e_1$, and $2e_1$ molecular orbitals, respectively. The denominators give the energy separation between the ground state and the two states connected to it by the spin–orbit coupling, and λ_{eff} is the effective spin–orbit coupling constant, which amounts

(13) Andrea, R. R.; Terpstra, A.; Oskam, A.; Bruin, P.; Teuben, J. H. *J. Organomet. Chem.* **1986**, *307*, 307.
(14) Rettig, M. R.; Drago, R. S. *J. Am. Chem. Soc.* **1968**, *91*, 3432.
(15) Fantucci, P.; Balzarini, P.; Valenti, V. *Inorg. Chim. Acta* **1977**, *25*, 113.

to 335 and 339 cm^{-1} for Zr^0 and Zr^+, respectively.[16] We do not know the exact charge of the metal, but we expect that it is about zero as in other parent compounds such as [CpTi(cot)]. The *b* and *c* coefficients are related by orthonormalization relations, but we ignore the d_{z^2} coefficient *a* in the ground state. It amounts to 0.96 in [CpTi(cot)] and lies between 0.95 and 0.97 in other parent compounds such as [CpTi(cht)], [CpV(cht)], and [CpCr(cht)].[17] If we take λ_{eff} = 335 cm^{-1}, a = 0.96, $E(1e_1) - E(a_1)$ = −24 100 cm^{-1}, and $E(2e_1) - E(a_1)$ = 17 600 cm^{-1}, the latter being the average value deduced from the two OA bands at 528 and 618 nm, we obtain b = 0.59 and c = 0.81. We may conclude that the empty $2e_1$ orbitals are essentially of metal character, but the $1e_1$ orbitals have also a significant metal character although the latter is only of 8.5% in [CpTi(cot)] $1e_1$ orbitals.[17] This high metal character of the $1e_1$ orbitals is also confirmed by the increased intensity of ionization from this orbital in He II versus He I photoelectron spectra.[13]

Conclusion. The above EPR and proton ENDOR studies show that the electron ground state of [Cp*Zr(cot)] is nonbonding and of essentially d_{z^2} character, as anticipated from MO calculations in this family of compounds. This is shown by the low spin density at protons resulting from a direct delocalization of the unpaired electron on the 1s hydrogen orbitals and confirmed by the negative spin density at $2p_z$ orbitals of Cp carbons. The inner e_1 orbitals are mainly of Cp character but they are more of metal character than in the Ti analogue. This implies that the real charge on the metal is close to zero.

The presence of methyl groups hinders the Cp ring rotation up to 100 K without affecting the (cot) rotation. This situation has already been observed with [(Me-Cp)Ti(η^8-C_8H_8)].[11]

The lack of resolution of zirconium satellites in the EPR spectrum precluded measurements of ^{91}Zr ENDOR. For this purpose, we are currently undertaking investigations on zirconium paramagnetic sandwich compounds where zirconium hyperfine lines are resolved so that these measurements can be performed.

Finally, although the results described above are in agreement with what is already known on compounds of similar structure and what is expected, they provide a basis for a model since the corresponding compound has been isolated and fully characterized. This is a rare case in zirconium chemistry. On the other hand, many Zr(III) compounds have been identified in solution on various occasions but could never be isolated; however, they usually give well-resolved EPR spectra. Their study by ENDOR on frozen solutions should therefore be easy and useful to provide additional information about their spatial and electronic configurations as shown in the present case.

Registry No. [Cp*Zr(cot)], 104389-95-9.

(16) Dunn, T. M. *Trans. Faraday Soc.* **1961**, *57*, 1441.
(17) Clack, D. W.; Warren, K. D. *Inorg. Chim. Acta* **1977**, *24*, 35.

Contribution from the Department of Chemistry and Center of Fundamental Materials Research, Michigan State University, East Lansing, Michigan 48824

Unanticipated Redox Transformations in Gold Polyselenides. Isolation and Characterization of $[Au_2Se_2(Se_4)_2]^{2-}$ and $[Se_{11}]^{2-}$

Mercouri G. Kanatzidis* and Song-Ping Huang

Received July 25, 1989

To date, soluble metal polyselenide chemistry has proven to be different from the corresponding metal polysulfide chemistry.[1] Although for a given metal polysulfide complex one might expect the analogous polyselenide or polytelluride complex to exist, the fact is that in most cases a different molecular structure or stoichiometry is adopted even under identical experimental conditions. Isostructural compounds containing all S_4^{2-}, Se_4^{2-}, and Te_4^{2-} ligands exist only in the divalent Ni and Zn groups of the periodic table[2-4] and in the Mo/Q_4^{2-} system.[5] This nonanalogous behavior can be attributed to (a) the significant variation of the chalcogen–chalcogen (Q–Q) bond as one moves from S to Te, resulting in considerably different Q_x^{2-} ligand sizes and (b) the differing reduction potentials required to split the various Q–Q bonds.[6] We have been exploring the chemistry of polyselenide and polytelluride ligands with late-transition metals and *p*-block elements because we believe that new structural motifs are possible and also that appropriate and interesting precursors to several useful chalcogenide semiconductors can be found. Interest in this aspect of polychalcogenide chemistry is intense.[7-9] Recently we reported[10] $[Ag(Se_4)]_n^{n-}$, a new one-dimensional polymer, and the discrete $[In_2(Se_4)_4(Se_5)]^{4-}$ ion.[11] In view of the absence of any known gold polyselenides and the fact that Ag^+ formed a very interesting polymeric structure, we set out to find analogous chemistry in the corresponding Au/Se_x system. Instead, we encountered a unique and curious set of redox reactions not previously observed in the Au/S_x or other M/Q_x systems. We report here the formation and structural characterization of two very interesting polychalcogenides, $[Se_{11}]^{2-}$ and $[Au_2Se_2(Se_4)_2]^{2-}$, that result from a remarkable interplay of electrons transferred from Au^+ to Se_x^{2-} and vice versa. We note that the $[Se_{11}]^{2-}$ anion has been synthesized and structurally characterized earlier by Krebs[12] (reported by Böttcher) but unfortunately no synthetic or accurate structural details are yet available. Two reproducible syntheses of $[Se_{11}]^{2-}$ are reported herein.

Experimental Section

All work was done in a glovebox (Vacuum Atmospheres, Inc.) under a nitrogen atmosphere. The solvents were stored over 4A Linde molecular sieves for several days and distilled under vacuum or a nitrogen

(1) (a) Wardle, R. W. M.; Bhaduri, S.; Chau, C.-N.; Ibers, J. A. *Inorg. Chem.* **1988**, *7*, 1747–1755. (b) Flomer, W. A.; O'Neal, S. C.; Cordes, A. W.; Jetter, D.; Kolis, J. W. *Inorg. Chem.* **1988**, *27*, 969–971. (c) Flomer, W. A.; O'Neal, S. C.; Pennington, W. T.; Jeter, D.; Cordes, A. W.; Kolis, J. W. *Angew. Chem., Int. Ed. Engl.* **1988**, *27*, 1702–1703. (d) Wardle, R. W. M.; Mahler, C. H.; Chau, C.-N.; Ibers, J. A. *Inorg. Chem.* **1988**, *27*, 2790–2795.
(2) Muller, A.; Schimansky, J.; Schimansky, U.; Bögge, H. *Z. Naturforsch.* **1985**, *40B*, 1277–1288.
(3) Adel, J.; Weller, F.; Dehnicke, K. *Z. Naturforsch.* **1988**, *43B*, 1094–1100.
(4) (a) Kanatzidis, M. G. *Abstracts of Papers*; 196th National Meeting of the American Chemical Society, Los Angeles, CA, 1988; INOR 469. (b) Dhingra, S.; Huang, S.-P.; Kanatzidis, M. G. Manuscript in preparation.
(5) (a) O'Neal, S. C.; Kolis, J. W. *J. Am. Chem. Soc.* **1988**, *110*, 1971–1973. (b) Draganjac, M.; Sihmon, E.; Chan, L. T.; Kanatzidis, M.; Baenziger, N. C.; Coucouvanis, D. *Inorg. Chem.* **1982**, *21*, 3321–3332. (c) Flomer, W. A.; Kolis, J. W. *Inorg. Chem.* **1989**, *28*, 2513–2517. (d) Ansari, M. A.; Mahler, C. H.; Ibers, J. A. *Inorg. Chem.* **1989**, *28*, 2669–2674.
(6) Cotton, F. A.; Wilkinson, G. *Advanced Inorganic Chemistry*, 5th ed.; Wiley: New York, 1988.
(7) (a) Steigerwald, M. L.; Rice, C. E. *J. Am. Chem. Soc.* **1988**, *110*, 4228–4231. (b) Steigerwald, M. L.; Sprinkle, C. R. *Organometallics* **1988**, *7*, 245–246. (c) Steigerwald, M. L.; Sprinkle, C. R. *J. Am. Chem. Soc.* **1987**, *109*, 7200–7201.
(8) (a) Haushalter, R. C.; Goshorn, D. P.; Sewchok, M. G.; Roxlo, C. B. *Mater. Res. Bull.* **1987**, *22*, 761–768. (b) Haushalter, R. C.; O'Connor, C. M.; Haushalter, J. P.; Umarji, A. M.; Shenoy, G. K. *Angew. Chem., Int. Ed. Engl.* **1984**, *23*, 169–170. (c) Haushalter, R. C.; O'Connor, C. M.; Umarji, A. M.; Shenoy, G. K.; Saw, C. K. *Solid State Commun.* **1984**, *49*, 929–933.
(9) (a) Molecular Design of Materials: Applications of Mechanistic and Structural Organometallic Chemistry. *Book of Abstracts*; 1987 Biennial Inorganic Chemistry Symposium, Harvard, University, Cambridge, MA. (b) Brinker, C. J.; Clark, D. W.; Ulrich, D. R. Better Ceramics Through Chemistry. In *Materials Research Society Symposia Proceedings*; Elsevier: New York, 1986; Vol. 73, and references therein.
(10) Kanatzidis, M. G.; Huang, S.-P. *J. Am Chem. Soc.* **1989**, *111*, 760–761.
(11) Kanatzidis, M. G.; Dhingra, S. *Inorg. Chem.* **1989**, *28*, 2024–2026.
(12) Böttcher, P. *Angew. Chem., Int. Ed. Engl.* **1988**, *27*, 759–772 (Krebs, private communication to Böttcher).

0020-1669/89/1328-4667$01.50/0